Unraveling the Gain Mechanism in High Performance Solution-Processed PbS Infrared PIN Photodiodes

*Jae Woong Lee, Do Young Kim, and Franky So**

High gain and low dark current solution-processed colloidal PbS quantum dots infrared (IR) PIN photodetectors with IR sensitivity up to 1500 nm are demonstrated. The low dark current is due to the P-I-N structure with both electron and hole blockers. The high gain in our IR photodiodes is due to the enhancement of electron tunneling injection through the 1,1-bis[(di-4-tolylamino) phenyl]cyclohexane (TAPC) electron blocker under IR illumination resulting from a distorted electron blocking barrier in the presence of photo-generated holes trapped in the TAPC electron blocker. It is further found that the trap states in the TAPC layer are generated by the Ag atoms penetrated in the TAPC layer during the thermal evaporation process. The resulting photodetectors have a high detectivity value of 7×10^{13} Jones, which is even higher than that of a commercial InGaAs photodiode.

1. Introduction

Infrared (IR) photodetectors have attracted a great deal of interest due to their applications in surveillance, range finding, and biomedical imaging as well as semiconductor wafer inspection.[1–4] Compound semiconductors such as InGaAs,[5] InSb,[6] and InAs/(GaIn)Sb superlattice[7] are commonly used for IR photodetector applications. However, expensive epitaxial techniques are typically used to grow these semiconductor materials, thus limiting their applications to small area devices. Recently, organic and/or solution-processed colloidal inorganic quantum dot (QD) materials for photodetectors have received a lot of attention because of their compatibility with low-cost large-area manufacturing.

High gain p–n junction-like photodiodes using organic and/or colloidal QD materials as the sensitizer have been demonstrated in the past.[8–10] The gain in these devices is mainly due to electron-trapped-induced charge injection at the organic/electrode interface. Further, most of these devices are primarily used in the visible wavelength range, and gain photodetectors for IR applications reported were mostly photoconductors with coplanar electrodes.[11] While first solution-processed PbS QDs Schottky junction gain photodiode in the IR wavelength (930 nm) was recently reported, the device showed a very small gain (<2).[12] In addition to gain, the dark current is another important device parameters to achieve high detectivities.[13–15] In the past, we demonstrated vertically stacked P-I-N like PbS QDs IR photodiodes with charge-blocking layers.[16] In photodiodes using organic and/or colloidal QD materials, these charge-blocking layers are inserted between the electrodes and the photoactive layer to reduce the dark current. More recently, we reported a vertically stacked P-I-N-like photodiode with multispectral response (visible to 1300 nm) and high detectivity (>10^{12} Jones) by using all solution-processed colloidal PbS QDs.[17] However, the detectivity of the IR photodiode is still lower than that of commercial InGaAs photodetectors because of their low responsivity even though they have very low noise currents. In this work, high gain and low dark current solution-processed colloidal PbS QDs IR PIN photodetectors with IR sensitivity up to 1500 nm are demonstrated. The low dark current is primarily due to the P-I-N structure with both electron and hole blockers to suppress carrier injection from the electrodes. The high gain in our IR photodiodes is due to the enhancement of electron tunneling through the 1,1-bis[(di-4-tolylamino) phenyl]cyclohexane (TAPC) electron blocker under IR illumination, resulting from a distorted electron-blocking barrier in the presence of photo-generated holes trapped in the TAPC electron blocker. We further found that the trap states in the TAPC layer are generated by the Ag atoms penetrated in the TAPC layer during the thermal evaporation process. Because of the high gain and low dark current, the resulting photodetectors have a high detectivity value of 7×10^{13} Jones, which is even higher than that of a commercial InGaAs photodiode.

2. Results and Discussion

2.1. Device Structure

Our IR photodiode shown in **Figure 1** has the following structure: indium tin oxide (ITO) as the cathode, ZnO nanocrystals (NCs) as the hole blocking layer (HBL), PbS QDs as the IR sensitizing layer, TAPC as the electron blocking layer (EBL), MoO_3 as the hole extraction layer (HEL), and Ag as the anode. PbS QDs used in our photodetectors have an absorption peak of 1200 nm. In order to improve the charge-transport properties of the PbS QD film, 1,3-benzenedithiol (BDT) was used as a capping ligand to provide surface passivation for the QDs while minimizing the spacing between them to facilitate carrier transport.[18] The Fermi level of PbS CQDs treated with BDT lies nearly at the midgap,[19] and therefore, the PbS QDs layer here can be treated as an intrinsic layer in the P-I-N like

Dr. J. W. Lee, Dr. D. Y. Kim, Prof. F. So
Department of Materials Science and Engineering
University of Florida
Gainesville, FL 32611, USA
E-mail: fso@mse.ufl.edu

DOI: 10.1002/adfm.201403673

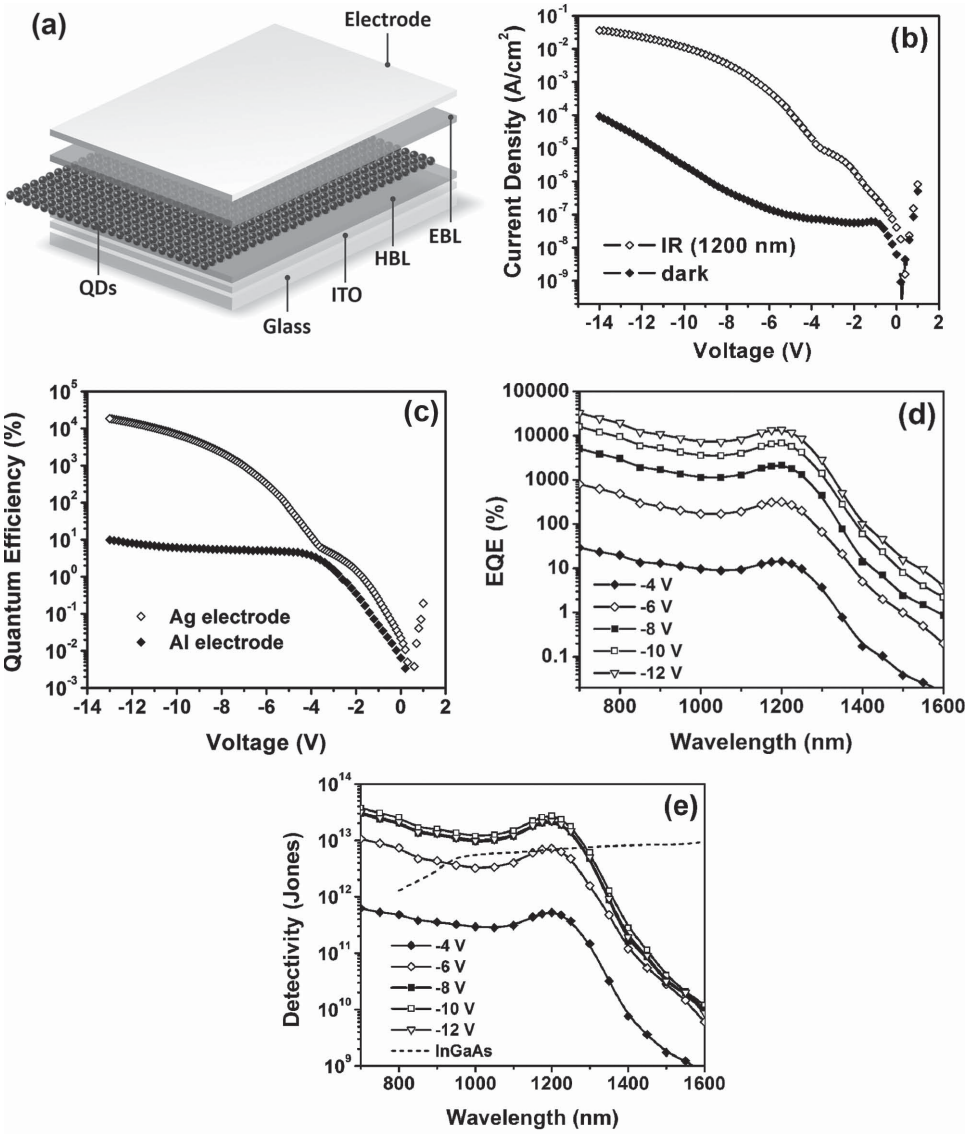

Figure 1. a) Schematic cross-section view of a gain PbS QD photodiode. b) *I–V* characteristics of a gain PbS QD photodiode under dark illumination and under illumination intensities of 165 μW cm^{-2}. c) External quantum efficiencies (at 295 K) of PbS QD photodiodes as a function of applied bias with Ag and Al electrodes. d) EQE values of a gain PbS QD photodiode as function of wavelength under reverse bias (at 295 K). The gain is obtained up to 1500 nm wavelength at –12 V. e) Detectivity values of a gain PbS QD photodiode as function of wavelength under reverse bias (at 295 K). The detectivity of InGaAs photodiode is taken from the literature.[20]

structure. To reduce the dark current, ZnO NCs with a large bandgap of 3.4 eV and a deep ionization potential of 7.6 eV are used as a hole blocking/electron transport layer (n-layer),[20–23] and a TAPC with a bandgap of 3.7 eV and a shallow lowest unoccupied molecular orbital (LUMO) energy of 1.8 eV is used as an electron blocking/hole transport layer (p-layer).

2.2. Photodetector with Solution-Processed PbS Nanoscrystals

2.2.1. Photodetector Characteristics

Figure 1b shows the current–voltage (*I–V*) characteristics of a typically IR photodiode in the dark and under 1200-nm illumination with a power density of 165 μW cm^{-2}. The *I–V* characteristics can be divided into two parts. At operating voltages up to –3.6 V, the device operates as a normal photodetector, and the photocurrent increases with increasing voltage and saturates at a reverse voltage of –2 V. The saturation in photocurrent at about –2 V indicates that most photo-generated carriers are being extracted. At reverse bias voltages above –3.6 V, however, the photocurrent begins to increase rapidly with increasing voltage and finally increases by three orders of magnitude at –13 V while the dark current increases by about two orders of magnitude over the same voltage range. The initial saturation in dark current indicates that the carrier-blocking layers suppress effectively the injection of charge carriers from both electrodes. However, at reverse bias voltages beyond –4 V,

the increase in dark current is due to carrier injection from the electrode and this point will be elaborated later.

The external quantum efficiency (EQE) as a function of the applied voltage for the reference device with an Al electrode as well as the device with a Ag electrode is shown in Figure 1c. The reference device with an Al anode operates as a normal photodetector and its EQE increases with the increasing voltage, then saturates at about 10% from –4 V up to –13 V. However, the EQE data for the device with a Ag anode can also be divided into two parts, similar to the *I–V* characteristics of the device. At voltages below –3.6 V, the EQE increases with increasing voltage and is saturated at about 10%, indicating that the device behaves as a normal photodetector similar to the reference device an Al electrode. As the reverse bias voltage increases further, the EQE increases again at –3.6 V, exceeding 100% at –5.2 V, and finally reaching a value of 18 700% at –13 V. The EQE spectra of the gain device under different wavelengths are also shown in the Figure 1d. The peak wavelength in the EQE spectra is 1200 nm, similar to the absorption spectrum of the PbS film. At an applied bias voltage of –12 V, the maximum EQE at the peak wavelength of 1200 nm is 13 800% and a gain of 1 is obtained even at 1500 nm. The gain in photodetectors with a similar photodiode structure has been attributed to interfacial trap-induced charge injection and the gain mechanism will be discussed in detail later in this paper.[8–10]

2.2.2. Analysis of the Photodetector Performance

In order to characterize performance of photodetectors, an important figure of merit in photodetectors is detectivity, *D** which is given by the following expression[24]

$$D^* = \left(A\Delta f\right)^{1/2} R / i_n \tag{1}$$

where A is the area of the detector in cm^2, Δf is the electrical bandwidth in Hz, R is the corresponding responsivity in A/W, and i_n is the noise current in Å. R is the responsivity which is determined using the following equation

$$R = \mathrm{EQE} \times \left(\frac{q}{h\upsilon}\right) \tag{2}$$

where q is the electronic charge, h is the Planck constant, and υ is the frequency of the incident photon. The noise current in the photodetector was measured using a Stanford Research SR830 lock-in amplifier and a SR570 low noise preamplifier.[11] During the measurements, the lock-in frequency of the noise current was set to be 30 Hz. In order to minimize the noise, the device was biased with alkaline batteries. Measurements were carried out in an electrically and optically shielded probe station. Figure 1e shows the detectivity spectra under different applied voltages. The detectivity spectra are also similar to the absorption spectrum of the PbS film, showing a peak wavelength of 1200 nm. At an applied voltage of –10 V, the detectivity is 2.6×10^{13} Jones at a wavelength of 1200 nm and 1.2×10^{11} Jones at a wavelength of 1500 nm. The detectivity decreases with increasing the applied bias beyond –10 V due to a significant increase of dark current. The detectivity value is even higher than that of a commercial InGaAs photodiode.[25]

2.2.3. Gain Mechanism in Photodetector

Understanding of the gain mechanism is a key to control the device parameters. To determine the gain mechanism in our photodetectors, devices with a Ag electrode were fabricated with different thicknesses of the ZnO HBL and the TAPC EBL. While the gain threshold voltage, at which the EQE begins to take off after saturation, is not affected by the thicknesses of the ZnO HBL, it is a strong function of the thickness of the TAPC EBL as shown in **Figure 2**a. Specifically, the gain threshold voltage increases significantly from –1.6 to –7.6 V with increasing thickness of the TAPC layer from 25 to 75 nm, respectively. It appears that the photocurrent gain is due to the TAPC layer. It is known that evaporation of Ag on organic materials results in penetration of Ag atoms leading to carrier traps. Here, we believe the gain is due to electron injection from the Ag electrode by tunneling through the TAPC EBL in the presence of trapped charges under IR illumination.

It is known that OLEDs with TAPC as a hole transporting layer have a short lifetime due to chemical changes during operation and chemical degradation in TAPC is coming from the weak carbon–nitrogen and carbon–carbon bonds in the amine group and the bond dissociation results in formation of free radicals and hole traps.[26] To prove the presence of trapped charges is due to the Ag layer, the following TAPC hole-only devices were fabricated: Device 1—ITO/TAPC (200 nm)/Al and Device 2—ITO/TAPC (50 nm)/Ag-doped TAPC (100 nm)/TAPC (50 nm)/Al, with the corresponding *I–V* characteristics shown in Figure 2b. In Device 1 with an Al anode, the current turn-on voltage is about –0.8 V, indicating a low hole injection barrier at the ITO/TAPC interface. Here, the hole current density increases rapidly from 3.4×10^{-9} A cm^{-2} at –0.8 V to 6.4×10^{-5} A cm^{-2} at –1.75 V. In order to understand the role of Ag played in the TAPC layer, first we tried to fabricate the device with the Ag anode: ITO/TAPC (200 nm) Ag^{-1}. However, this device shows a large dark current of about 1×10^{-1} mA cm^{-2} at a reverse bias of –0.5 V, indicating that the TAPC hole-only device is electrically shorted due to the penetration of Ag atoms, and this is a commonly known problem encountered in Ag evaporation.[27–30] To alleviate this shorting problem, Device 2 with a 10% Ag-doped TAPC sandwiched between the two undoped TAPC layers was fabricated. In this device, Al is used as the electrode. Based on the data from Device 1, we expect the trap density at the TAPC/Al interface should be low and electron injection from the Al electrode should be negligible. As shown in Figure 2b, there is no significant increase in current with a reverse voltage up to –1.75 V, indicating strong carrier trapping due to that Ag atoms in the TAPC layer.

To further verify the gain mechanism due to trap states generated by penetration of Ag atoms into the TAPC layer, the PbS IR photodiodes were fabricated with a Ag layer thickness varying from 0 to 100 nm. It should be noted that a 100-nm thick Al layer is deposited on top of the Ag layer to ensure good conductivity of the electrode for devices with a very thin Ag layer. Figure 2c shows the gain as a function of Ag layer thickness. It is apparent that the gain is a step function of the Ag layer thickness. Below a thickness of 20 nm, there is no gain in the detector. Above 20 nm, the detector gain jumps abruptly to about 50 and saturates at about 60 with increasing the Ag

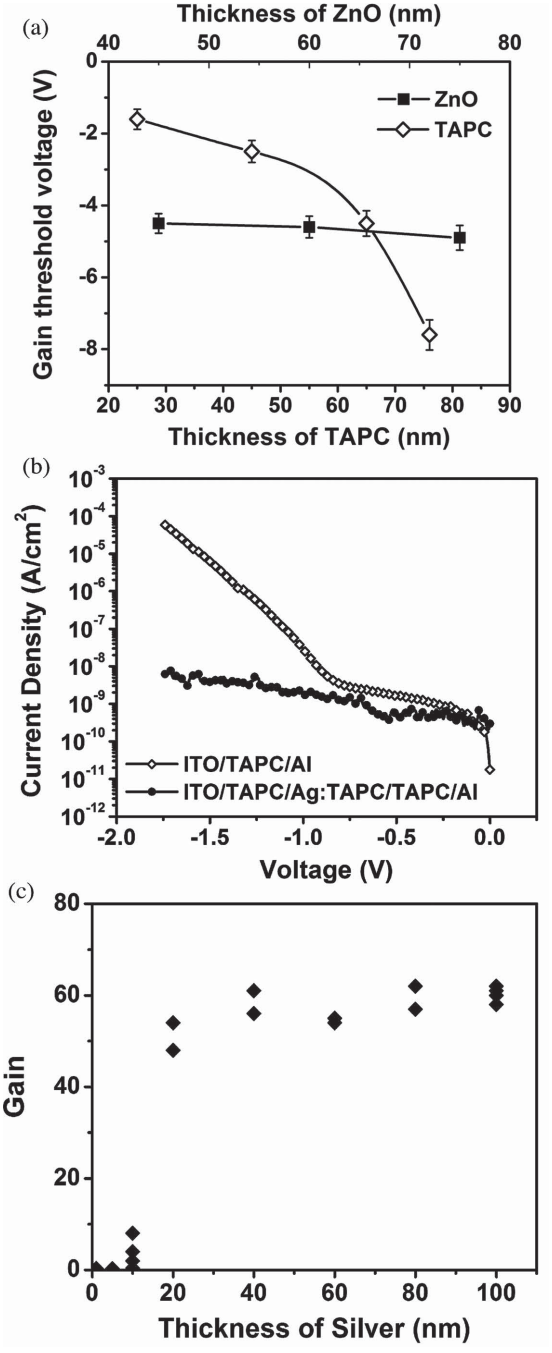

Figure 2. a) The change of gain threshold voltage according to the ZnO and TAPC thickness. b) *I–V* characteristics of three hole-only devices: (1) ITO/TAPC/Al and (2) ITO/TAPC/ Ag:TAPC/TAPC/Al devices. c) The gain as a function of Ag layer thickness.

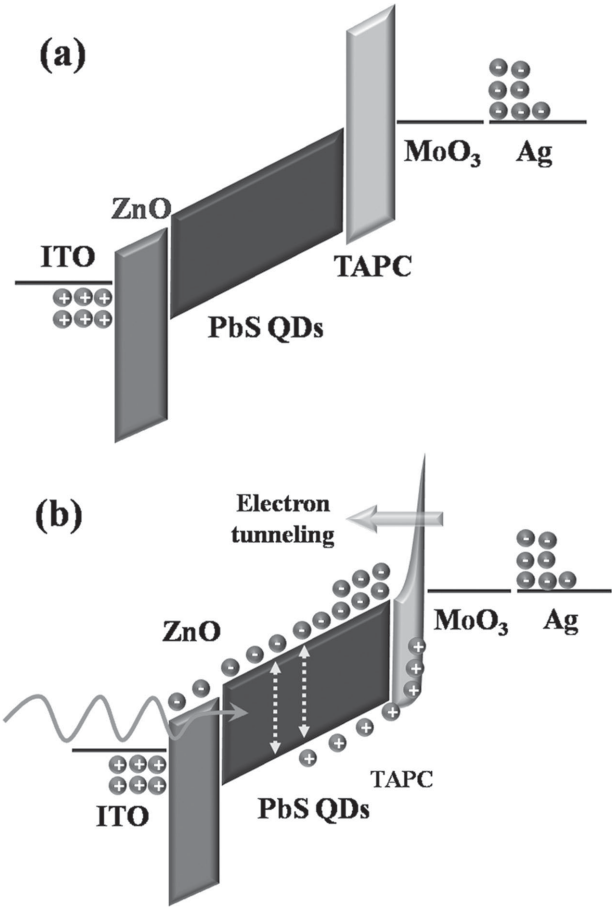

Figure 3. Schematic energy band diagrams of a gain PbS QD photodiode a) in the dark and b) in the IR illumination.

layer thickness, indicating that a critical dosage is required to generate the carrier traps. Therefore, these results confirm that penetration of Ag atoms onto the TAPC layer during the Ag evaporation generates hole traps in the TAPC EBL, leading to electron tunneling under the IR illumination.

Figure 3a,b shows the schematic band diagrams illustrating the gain mechanism of our IR photodetectors. In spite of using PbS QDs with the narrow bandgap of 1.03 eV, the gain photodetector has a low dark current under reverse bias due to the presence of both the hole and electron-blocking layers as illustrated in Figure 3a. Under IR illumination as illustrated in Figure 3b, photo-generated charge carriers in the PbS QDs layer move along the potential gradient under reverse bias. While photo-generated electrons are easily swept away through the ZnO layers, photo-generated holes are captured at the trap sites due to the penetration of Ag atoms into the TAPC layer. Accumulation of trapped holes in the TAPC layer builds up a high electric field at the TAPC/MoO_3 Ag^{-1} interface and distorts the electron injection barriers of the TAPC EBL, resulting in electron tunneling through the barrier from the Ag electrode as illustrated in Figure 3b.

2.2.4. Power Dependence of the Photodetector Performance

To further characterize the devices, we further measured the illuminated IR power dependence of the device as shown in **Figure 4**a,b. The gain in the photodetector decreases rapidly with increasing the intensity of illumination. At low light intensities, most of the photo-generated holes are trapped at the TAPC Ag^{-1} interface and greatly enhances electron injection from the Ag electrode. As the light intensity increases, a smaller fraction of the photo-generated holes are trapped and

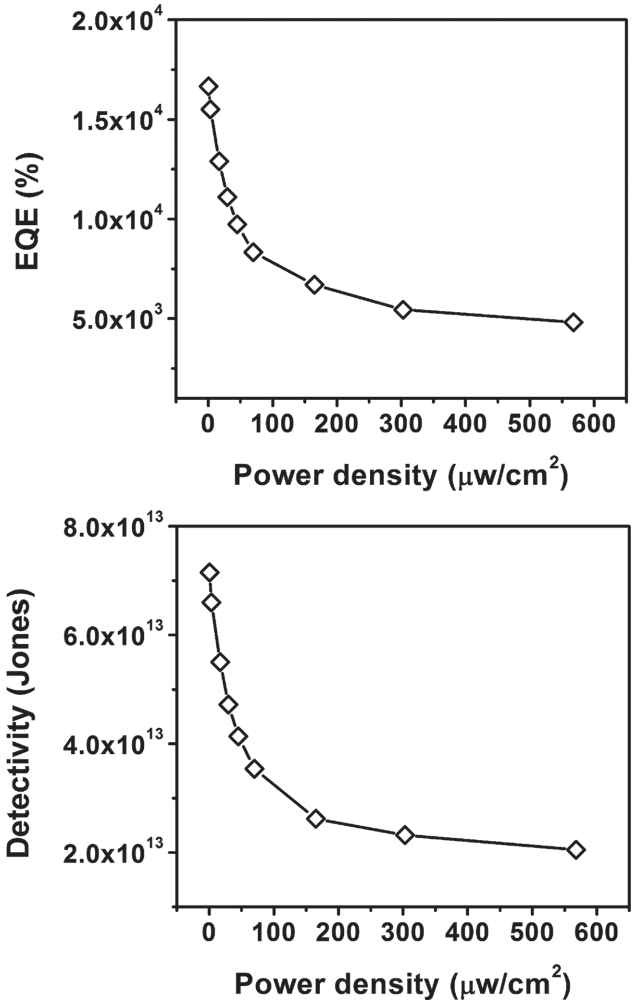

Figure 4. Light-intensity dependence of the a) EQE and b) detectivity with a constant bias 10 V applied.

hence the enhancement in electron injection from the Ag electrode decreases, resulting in a smaller gain with increasing light intensity. With an IR intensity higher than 300 μW cm^{-2}, therefore, the detectivity and EQE at –10 V are saturated to 2×10^{13} Jones and 5000%, respectively. The highest detectivity of 7.0×10^{13} Jones and the highest EQE of 16 000% were obtained at an intensity of 0.5 μW cm^{-2}. While there are several reports in visible and ultraviolet photodetectors with similar gain dependence on the irradiated light power densities,[31] this is a first report on the IR photodiodes with a high responsivity (>5000%) over a wide range of light intensities (<550 μW cm^{-2}).

2.2.5. Response Time

Another important parameter in the photodetectors is the response time. **Figure 5** shows the transient photocurrent of the gain photodetector under IR illumination. We define the rise time to be the time it takes the photocurrent to reach 63.2% of the saturated photocurrent from the dark current at the rising edge and the fall time to be the time it takes to fall to 36.8%

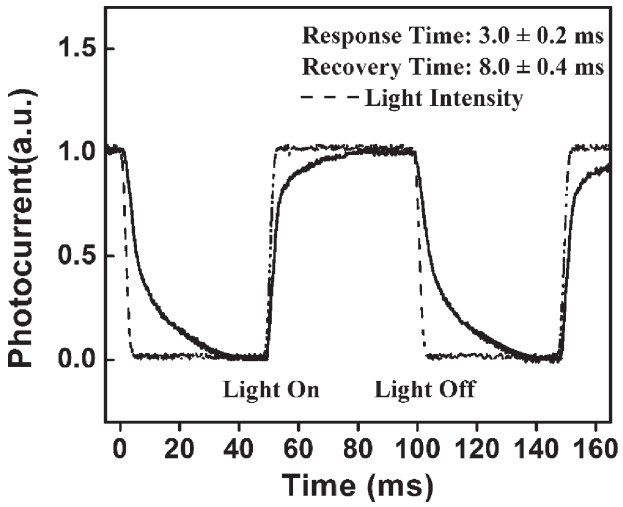

Figure 5. Transient photo response of a gain PbS QD photodiode with 28 gain.

of the saturated photocurrent. Here, we obtain a rise time of 3.0 ± 0.2 ms and a fall time of 8.0 ± 0.4 ms. The fall time is slower than the rise time, indicating that the release time of the trapped holes is slower than the trapping time of the photogenerated holes. Our gain photodiodes have sufficient speed for imaging applications with more than 10× higher detectivity and 100× higher responsivity compared with commercially available IR photodetectors.[32,33]

3. Conclusion

The solution-processed PbS QD photodiode are fabricated with an IR sensitivity up to 1500 nm. At a peak wavelength of 1200 nm, the photodetector has a gain of 187, a detectivity of 7.0×10^{13} Jones, and a response time of 3.0 ± 0.2 ms. The gain in the photodetector is due to the enhancement of electron injection through the TAPC EBL under IR illumination, resulting from hole traps generated by Ag evaporation onto the TAPC layer. Due to the higher detectivity than commercial InGaAs photodetector, the sufficient response time for imaging applications, and the potentially low-cost fabrication process, this kind of IR photodetectors is promising for low-cost IR sensing applications.

4. Experimental Section

Synthesis of ZnO Nanocrystals: The synthesis has been previously published.[34,35] For the hole-blocking layer, we used ZnO NCs ranging from 3 to 5 nm in size, which were synthesized by dropwise addition of a stoichiometric amount of tetramethylammonium hydroxide (TMAH) (0.55 M) to 30 mL of 0.1 M zinc acetate dihydrate dissolved in dimethyl sulfoxide (DMSO) under continuous stirring. After precipitation and washing, the nanoparticles were dissolved in ethanol and stored under ambient conditions. All solutions were filtered with a 0.45 μm filter.

Synthesis of PbS Nanocrystals: The synthesis has been previously published.[17] In a typical reaction, 0.888 g of PbO (Sigma-Aldrich) was dissolved with 6 mmol of oleic acid in a three-necked flask under Ar flow with 50 mL of octadecene (ODE). The solution was heated and held at 130 °C. 360 μL of hexmethyldisathiane ($(TMS)_2S$) (Sigma-Aldrich) was

dissolved in 5 mL of ODE and injected into three necked flasks. The reaction continued for 5 min. To terminate the reaction, cold toluene was injected into the reaction mixture. The resulting nanocrystals were subsequently washed via precipitation with a polar solvent such as acetone and redispersion in toluene, and the process was repeated 3×.

Device Fabrication: Devices were fabricated on patterned ITO substrates with a sheet resistance of less than 20 Ω^{-2}. The ITO substrates were first cleaned with acetone and isopropanol in an ultrasonic cleaner and subsequently rinsed with deionized water, blown dry with N_2 gas, and treated with UV ozone. Following this, a 60-nm layer of ZnO nanocrystals was spin-coated on top of the ITO substrate and then annealed at 90 °C for 15 min in the ambient. The substrate was subsequently introduced into a nitrogen glovebox. The cross linked PbS QDs thin films were fabricated with a sequential layer by layer spin casting method. Multiple PbS QDs layer was then treated with a 1,3-benzenedithiol (BDT) following the same procedure described in our previous work[14,17] to improve electronic coupling between individual nanocrystals. This treatment renders the PbS film insoluble. 1,1-Bis[(di-4-tolylamino) phenyl]cyclohexane (TAPC) and Ag/Al layers in the devices were vacuum deposited at a pressure of 1×10^{-6} Torr. The deposition rates were 0.9 Å s^{-1} and 1.0 Å s^{-1} for organic materials and Ag/Al electrodes, respectively. The area of the device is 0.04 cm^2.

Device Characterization: All characterization and noise measurements were performed at room temperature. Current–voltage (*J–V*) characterization was measured with a Keithley 4200 semiconductor parameter analyzer system connected to a calibrated Si and Ge photodiode (Newport) for photocurrent measurement. EQE and responsivity measurements were conducted using an in-house setup consisting of a Xenon DC arc lamp, an ORIEL 74125 monochromator, a Keithley 428 current amplifier, an SR 540 chopper system, and an SR830 DSP lock-in amplifier from SRS. The intensity of the incident irradiation was varied by using a set of neutral density filters and a diffuser.

Acknowledgements

The authors gratefully acknowledge financial support for the research from Nanoholdings.

Received: October 20, 2014
Revised: November 21, 2014
Published online: January 21, 2015

[1] P. W. Kruse, F. C. Pribble, R. G. Schulze, *J. Appl. Phys.* **1967**, *38*, 1718.
[2] Y. Mita, *Appl. Phys. Lett.* **1981**, *39*, 587.
[3] Y. H. Wang, J. Ohwaki, *J. Appl. Phys.* **1993**, *74*, 1272.
[4] K. J. Russell, I. Appelbaum, H. Temkin, C. H. Perry, V. Narayanamurti, M. P. Hanson, A. C. Gossard, *Appl. Phys. Lett.* **2003**, *82*, 2960.
[5] R. W. M. Hoogeveen, R. J. van der A, A. P. H. Goede, *Infrared Phys. Technol.* **2001**, *42*, 1.
[6] R. D. Thom, T. L. Koch, J. D. Langan, W. J. Parrish, *IEEE Trans. Electron Dev.* **1980**, *27*, 160.
[7] D. L. Smith, C. Mailhiot, *J. Appl. Phys.* **1987**, *62*, 2545.
[8] M. Hiramoto, T. Imahigashi, M. Yokoyama, *Appl. Phys. Lett.* **1994**, *64*, 187.
[9] H. Y. Chen, M. K. F. Lo, G. W. Yang, H. G. Monbouquette, Y. Yang, *Nat. Nanotechnol.* **2008**, *3*, 543.
[10] Y. Kim do, J. Ryu, J. Manders, J. Lee, F. So, *ACS Appl. Mater Interfaces* **2014**, *6*, 1370.
[11] G. Konstantatos, I. Howard, A. Fischer, S. Hoogland, J. Clifford, E. Klem, L. Levina, E. H. Sargent, *Nature* **2006**, *442*, 180.
[12] R. Dong, C. Bi, Q. F. Dong, F. W. Guo, Y. B. Yuan, Y. J. Fang, Z. G. Xiao, J. S. Huang, *Adv. Opt. Mater.* **2014**, *2*, 549.
[13] B. N. Pal, I. Robel, A. Mohite, R. Laocharoensuk, D. J. Werder, V. I. Klimov, *Adv. Funct. Mater.* **2012**, *22*, 1741.
[14] G. Sarasqueta, K. R. Choudhury, F. So, *Chem. Mater.* **2010**, *22*, 3496.
[15] J. P. Clifford, G. Konstantatos, K. W. Johnston, S. Hoogland, L. Levina, E. H. Sargent, *Nat. Nanotechnol.* **2009**, *4*, 40.
[16] G. Sarasqueta, K. R. Choudhury, J. Subbiah, F. So, *Adv. Funct. Mater.* **2011**, *21*, 167.
[17] J. R. Manders, T-H. Lai, Y. An, W. Xu, J. Lee, D. Y. Kim, G. Bosman, F. So, *Adv. Funct. Mater.* **2014**, *24*, 7205.
[18] H. Y. Fu, S. W. Tsang, Y. G. Zhang, J. Y. Ouyang, J. P. Lu, K. Yu, Y. Tao, *Chem. Mater.* **2011**, *23*, 1805.
[19] P. R. Brown, D. Kim, R. R. Lunt, N. Zhao, M. G. Bawendi, J. C. Grossman, V. Bulovic, *ACS Nano* **2014**, *8*, 5863.
[20] G. Sarasqueta, K. R. Choudhury, J. Subbiah, F. So, *Adv. Funct. Mater.* **2011**, *21*, 167.
[21] P. P. Boix, J. Ajuria, R. Pacios, G. Garcia-Belmonte, *J. Appl. Phys.* **2011**, *109*, 074514.
[22] D. C. Lim, W. H. Shim, K. D. Kim, H. O. Seo, J. H. Lim, Y. Jeong, Y. D. Kim, K. H. Lee, *Sol. Energy Mater. Sol. Cells* **2011**, *95*, 3036.
[23] D. Y. Kim, K. R. Choudhury, J. W. Lee, D. W. Song, G. Sarasqueta, F. So, *Nano Lett.* **2011**, *11*, 2109.
[24] G. Konstantatos, *Colloidal Qquantum Dot Optoelectronics and Photovoltaics*, Cambridge University Press, UK **2013**.
[25] X. Gong, M. H. Tong, Y. J. Xia, W. Z. Cai, J. S. Moon, Y. Cao, G. Yu, C. L. Shieh, B. Nilsson, A. J. Heeger, *Science* **2009**, *325*, 1665.
[26] D. Y. Kondakov, *J. Appl. Phys.* **2008**, *104*, 084520.
[27] S. Scholz, Q. Huang, M. Thomschke, S. Olthof, P. Sebastian, K. Walzer, K. Leo, S. Oswald, C. Corten, D. Kuckling, *J. Appl. Phys.* **2008**, *104*, 104502.
[28] M. Scharnberg, J. Hu, J. Kanzow, K. Ratzke, R. Adelung, F. Faupel, J. Pflaum, *Defect Diffus. Forum* **2005**, *237–240*, 993.
[29] M. Scharnberg, J. Hu, J. Kanzow, K. Ratzke, R. Adelung, F. Faupel, C. Pannemann, U. Hilleringmann, S. Meyer, J. Pflaum, *Appl. Phys. Lett.* **2005**, *86*, 024104.
[30] J. H. Cho, D. H. Kim, Y. Jang, W. H. Lee, K. Ihm, J. H. Han, S. Chung, K. Cho, *Appl. Phys. Lett.* **2006**, *89*, 132101.
[31] G. Konstantatos, J. Clifford, L. Levina, E. H. Sargent, *Nat. Photonics* **2007**, *1*, 531.
[32] A. Rogalski, *Prog. Quant. Electron.* **2003**, *27*, 59.
[33] H. C. Liu, *Opto-Electron. Rev.* **2003**, *11*, 1.
[34] M. Hartel, S. Chen, B. Swerdlow, H. Y. Hsu, J. Manders, K. Schanze, F. So, *ACS Appl. Mater. Inter.* **2013**, *5*, 7215.
[35] J. H. Hu, R. G. Gordon, *J. Appl. Phys.* **1992**, *71*, 880.